Chapter 2
Growth and Properties of Bulk AlN Substrates

Matthias Bickermann

Abstract Bulk crystal growth of aluminum nitride (AlN) comes into focus in order to provide substrates for deep-UV optoelectronics (LEDs, lasers, and sensors) which are typically based on Al-rich AlGaN epitaxial layers and structures. On AlN substrates, pseudomorphic AlGaN layers can be deposited with compressive strain and high structural quality [1–3]. In this context, the growth of AlN crystals by sublimation and recondensation (physical vapor transport method) at temperatures exceeding 2000 °C has proven to be the method of choice, as the boules and substrates show very high structural perfection at reasonable growth rates. Availability of AlN substrates as well as their useable area, structural quality, and electrical/optical properties are directly related to growth technology issues, including selection of set-up materials, seeding strategy, and pre-purification efforts. After a brief overview of history and applications of bulk AlN, the basic principles of AlN bulk growth by physical vapor transport (PVT) are reviewed. The formation of extended defects and the incorporation of impurities during growth as well as their impact on the material's optical and electrical properties are discussed in detail. The main target of this chapter is to provide readers with enough information about AlN substrate preparation to understand and make informed decisions about employing AlN substrates for deep-UV optoelectronics.

2.1 Properties and History of AlN Crystals

AlN is a binary compound crystallizing in the hexagonal wurtzite structure ($P6_3/mmc$). Each atom is surrounded by a regular tetrahedron of atoms of the other kind. The ionic fraction of the chemical bond is 42 % [4]. The sp^3 bonding in conjunction with

M. Bickermann (✉)
Leibniz Institute for Crystal Growth (IKZ), Berlin, Germany
e-mail: matthias.bickermann@ikz-berlin.de

M. Bickermann
Institute for Chemistry, Technische Universität, Berlin, Germany

M. Kneissl and J. Rass (eds.), *III-Nitride Ultraviolet Emitters*,
Springer Series in Materials Science 227, DOI 10.1007/978-3-319-24100-5_2

the low atomic mass of its constituents leads to extraordinary high chemical stability, phonon energies (around 100 meV), bulk acoustic wave velocities (11270 m/s), and thermal conductivity (about 320 W/mK) [5, 6]. AlN crystals are polar, birefringent, pyroelectric, and piezoelectric.

The high chemical stability imposes a considerable challenge to crystal growth. AlN decomposes before melting under technologically feasible conditions [7]. Thus, growth from the melt, as performed for most other III–V semiconductors, is not possible. On the other hand, the total pressure of gaseous species above the solid already reaches considerable values much below the decomposition temperature (about 2430 °C at 1 bar total pressure). This sublimation can be used to facilitate a species transport, mediated, e.g., by a concentration gradient which is induced by a temperature gradient, from the hotter source to the colder growth area, where the species condense to form a crystal. The corresponding process of high-temperature sublimation and recondensation is called physical vapor transport (PVT). The PVT method is employed also for bulk SiC growth, where it was developed into an industrial technique.

Today, bulk AlN crystals are almost exclusively grown by PVT. Alternative growth methods like high-temperature chemical vapor deposition (HT-CVD/HVPE) [8–11], thermal decomposition [12], PVT variations using the sandwich sublimation method [13], or liquid Al as precursor [14] as well as high-temperature solution, flux, and ammonothermal growth [15–20] are also investigated for bulk growth, but currently remain at a research level due to unresolved restrictions in crystal size, growth rate, or yield. On the other hand, preparation of an HVPE layer on an AlN bulk substrate with subsequent removal of that substrate is currently proposed to provide a UV-transparent template suitable for light out-coupling [21].

Aluminum nitride (AlN) was first synthesized in 1862 by reacting molten aluminum with nitrogen gas [22]. Today, AlN powder is mainly synthesized from alumina by carbothermal nitridation [23]

$$Al_2O_3 + 3\,C + N_2 \rightarrow 2AlN + 3\,CO. \tag{2.1}$$

AlN ceramics are used as refractory construction parts, heat sinks, and substrates where high thermal conductivity is required in conjunction with high mechanical and thermal robustness [24, 25]. However, due to the high preparation cost compared to alumina, the use of AlN ceramics remains restricted to high-end products and niche markets.

The first serious attempts to grow bulk AlN single crystals date back to the 1960s [26–30]. AlN, powder or liquid, Al were used as source materials in an atmosphere of nitrogen at temperatures exceeding 1700 °C. The experiments were conducted in carbon-containing set-ups, which led to highly contaminated crystals. In 1976, Slack and McNelly prepared mm-sized AlN single crystals with high purity [7, 31, 32] by using a Piper-Polich [33] growth technique in which a sealed rhenium/tungsten crucible with conical end was moved through a hot zone of an inductively heated furnace. However, research on AlN bulk single crystal growth

for epitaxial substrate preparation only started in the late 1990s [34–36] with the rising interest in wide band-gap semiconductors. The reactor design from the much more advanced SiC PVT technique [37], in which SiC sublimates and condenses at temperatures 2100–2500 °C in graphite crucibles was soon adopted for AlN growth. However, a lot of initial work was dedicated to find chemically stable and suitable hot-zone materials [38–41]. Also, the initial absence of AlN seeds led to different strategies to obtain large bulk of single crystals [42].

As of today, a few companies and research facilities have demonstrated AlN single crystals of up to 2 in. in diameter [43–49]. Worldwide AlN substrate production is still very small as compared to SiC or sapphire. While the main target is still to produce substrates for UV optoelectronics [50–56], other potential applications for AlN bulk crystals, including piezo- and pyroelectrics, electroacoustics [57], and substrates for AlGaN-based power devices [58, 59] are currently evaluated.

2.2 AlN Bulk Growth by the PVT Method: Theory

In the thermodynamic Al–N [60] system, the only stable compounds are Al, AlN, and N_2, see Fig. 2.1a. At temperatures and pressures relevant for crystal growth and under nitrogen excess, only gaseous Al and N_2 are at equilibrium with solid AlN. Other species are calculated to appear at much lower concentrations [61], and their

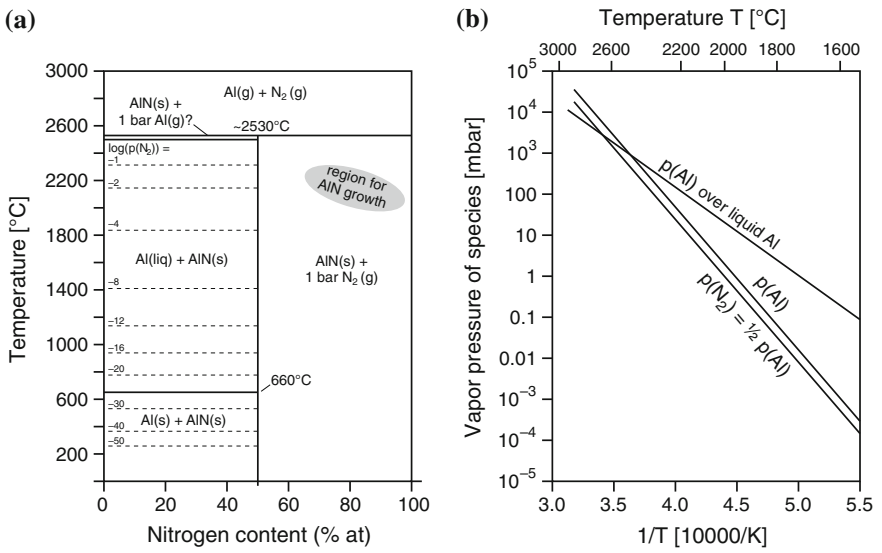

Fig. 2.1 **a** Phase diagram at 1 bar (with N_2 fugacities, after [60], and the region for AlN growth) and **b** partial pressure of vapor species under stoichiometric sublimation in the Al–N_2 system with Al partial pressure over liquid Al (after [7])

relevance for crystal growth is considered negligible. Thus, the sublimation–recondensation reaction can be written as

$$2\,\mathrm{AlN(s)} \rightleftharpoons 2\,\mathrm{Al(g)} + \mathrm{N_2(g)} \tag{2.2}$$

with the equilibrium constant $K = \mathrm{e}^{-\Delta G/RT} = p_{\mathrm{Al}} \cdot p_{\mathrm{N2}}^{1/2}$, $\log_{10} K = -32450/T + 16.08$ [62]. $\Delta G \approx 630$ kJ/mol [63] is the Gibbs free energy for sublimation, R is the universal gas constant, T is the temperature, and p_{Al} and $p_{\mathrm{N2}} = ½\, p_{\mathrm{Al}}$ are the temperature-dependent equilibrium partial pressures of the gaseous products [7], see Fig. 2.1b.

In contrast to melt growth where the growth temperature is determined by the melting temperature of the compound, sublimation growth can be performed generally at any temperature. In sublimation growth, a temperature difference ΔT between source and seed provides for a net mass flow rate of species J_{Transp} through the growth space due to the concentration gradients formed by the temperature-dependent partial pressures. The Al partial pressure over AlN provides sufficient evaporation for mass transport even at 1600 °C, but due to insufficient surface ad-atom mobility and/or N_2 chemical activity, only very thin needles form at this temperature [62]. Higher temperatures are beneficial for increasing both growth rate and surface kinetics, i.e., helping the atoms to properly arrange themselves at the surface. But in any case, the concentration of species in the gas phase is in the orders of magnitude lower than in melt growth, which restricts the achievable growth rate.

Stoichiometric sublimation ("into vacuum") results in very high deposition rates and polycrystalline growth due to lack of growth control. Instead, the transport and deposition during growth is regulated by buffering with N_2 "in excess," i.e., adding N_2 to the growth atmosphere so that the total pressure in the system p_{sys} is about 2–10 times higher than the total pressure of vapor species. As a consequence, in the gas phase, $N_{\mathrm{Al}}/N_{\mathrm{N}} = p_{\mathrm{Al}}/(2 \cdot p_{\mathrm{sys}})$ is in the order of 0.1. While excess N_2 does not necessarily lead to N-rich growth conditions, this is the commonly assumed growth regime for AlN growth (AlN–N_2 system). The growing AlN crystal still enforces stoichiometry, as its existence range is confined, but might form vacancies. The chemical activity of N_2 is most probably governed by kinetics of surface reactions such as [62]

$$\mathrm{Al(ads)} + \mathrm{N_2(ads)} \rightleftharpoons \mathrm{AlN(s)} + \mathrm{N(ads)}. \tag{2.3}$$

Additionally, nitrogen dissociation could be enhanced via reaction with impurities.

In AlN sublimation growth models, sublimation and recondensation are typically described by Hertz–Knudsen equations as

$$J_{\mathrm{Subl/Recond}} = \alpha \cdot (2\pi\, mRT)^{-1/2} \cdot \Delta p \tag{2.4}$$

with α as the (effective) sublimation/condensation coefficient, m as the molar mass, and Δp as the difference between the actual (super- or undersaturated) and the

equilibrium partial pressure of the transported species at the source or seed area, respectively. Assuming Al as the rate-limiting species, as N_2 is provided in excess [62], it is sufficient to regard only Al species, and α is typically set to unity for AlN growth.

It is commonly assumed that the mass transport in the gas phase is dominated by diffusion (Fick's law). Natural convection is typically absent at the given growth conditions (cf. [64]), and advection (Stefan flow) is insignificant due to the N_2 buffering. If the limiting step for bulk growth is indeed diffusive mass transport, i.e., sublimation or recondensation kinetics are considerably faster than diffusion in the vapor phase, the growth rate R_G can be approximated by [63, 65]

$$R_G = J_{Transp}\, m_{AlN}/\rho_{AlN} \propto (\Delta T/L) \cdot e^{-\Delta G/RT}/(T^{1.2} \cdot p_{sys}^{1.5}). \tag{2.5}$$

with m_{AlN} and ρ_{AlN} as the mass and density of solid AlN, and L as the source-to-seed distance.

The parameters governing the mass transport are thus T, p_{sys}, and $\Delta T/L$. The growth rate increases with increasing temperature gradient and temperature (due to the exponential term), while the increase with decreasing total pressure is in fact rather weak for typical growth conditions [66]. In the practical case, R_G is lower due to volatile species leaving the semi-open crucible and reacting with the crucible materials. Finally, the presence of impurities may significantly change growth behavior, e.g., via impurity-assisted transport of growth species, or by acting as surfactants, i.e., changing kinetic barriers at the growth surface [67–69]. As a consequence, preparation of highest purity source materials is not only mandatory in order to control the properties of the grown crystals, it is also necessary for achieving a stable and reproducible crystal growth.

As mentioned, AlN bulk growth is typically performed at temperatures T ranging from 1800 to 2300 °C and system pressures p_{sys} of 300–900 mbar. The process window for stable growth of AlN depends on the hot-zone and seed materials (see below) and the growth orientation (polarity). Higher temperatures and supersaturations seem to stabilize N-polar growth [70, 71]. As only a relatively low growth rate R_G (typically lower than 200 µm/h) will allow for single-crystalline growth without deterioration of structural quality, the axial thermal gradients $\Delta T/L$ are typically in the range of only 2–10 K/cm.

2.3 AlN Bulk Growth by the PVT Method: Technology

The hot-zone of the typically used vertical set-up consists of a cylindrical crucible with removable upper lid where a seed can be mounted, a surrounding susceptor, and thermal insulation, see Fig. 2.2. The crucible has to be porous or semi-closed to allow gas and pressure exchange with the environment, often provided already by the nonideal closure between the lid and the crucible. It is filled with solid AlN source material (as powder, sintered bodies, or lumps from previous growth

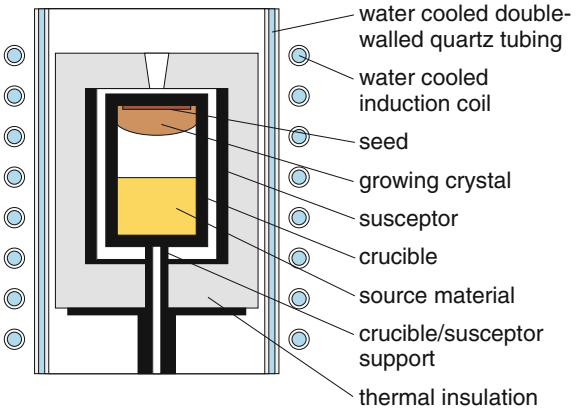

Fig. 2.2 Crucible and reactor set-up for AlN bulk growth

experiments) to 50–80 % of its total height. The hot-zone geometry has to be carefully designed to provide the proper thermal gradients at growth temperatures, where heat is dominantly transferred by radiation.

Electrical power is used to heat the crucible either by induction (at 8–50 kHz frequency, depending on the susceptor material) or by resistive heating, whereas the former is much more established. The use of a susceptor is advantageous in that it remits the heat to the crucible via radiation, providing a more homogeneous temperature field in the growth cell compared to direct crucible heating. As shown in Fig. 2.2, the set-up is located inside a water-cooled growth vessel which provides the gas-tight enclosure, a loading port, and connections for pyrometer access and gas inlet/outlet. Some reactors allow for a controlled movement of the coil relative to the crucible to affect the axial temperature gradient in the crucible; this can be also facilitated by separate control of several heaters.

The growth procedure typically includes the following steps: The hot-zone is assembled and loaded into the reactor. After purging and pre-heating steps, the vessel is filled with N_2 gas, and the growth cell is heated to growth temperature. During heating up, the seed is kept at a slightly higher temperature than the source material to prevent early growth, clean the seed surface, and further remove volatile impurities. If the growth temperature is reached, a soft growth start is achieved by inverting the axial temperature gradient, i.e., providing a higher temperature at the source compared to the seed. During growth, the system pressure is kept constant by maintaining a constant inert gas input flow while controlling the exhaust flow.

As the temperature inside the growth cell is inaccessible, the "growth temperature" is obtained by pyrometers measuring the temperatures of crucible outer surfaces (e.g., on the upper and lower lid) and controlled by adjusting the heating power. Note that maintaining the temperature gradients at the growth interface during growth is crucial in order to obtain crystals with high chemical and structural homogeneity. Thus, the thermal gradients near the growing surface during growth are derived by numerical modeling. The gradients depend on the complete hot-zone geometry including radiation shields and thermal insulation (for which accurate

material data at growth temperatures is rarely available) and on the growth rate (due to release of latent heat), and transient simulations are needed to account for the move of the growth interface while the boule grows.

Considering the typical growth rates of 50–300 µm/h, it takes several days to grow 10–30 mm thick crystals. Mass transport yields exceeding 80 % are possible if the evaporation losses through the semi-open crucible are kept at a low level. The end of growth is initiated by decreasing the heater power, optionally with inverting the gradient again. A controlled cooling is demanded to mitigate strain-induced defect formation.

As will be shown below, the selection of hot-zone materials has a decisive impact on AlN growth behavior and properties. Typically, the crucible is made from either tungsten (W) or tantalum carbide (TaC). Graphite and boron nitride lead to considerable contamination of the crystal with carbon or boron, respectively; a few more materials have been positively evaluated (Re [7], TaN, HfN, TaB_2), but are not currently used [38–41]. Tungsten is long-term stable against Al vapor in the presence of sufficient N_2, and chemical erosion is negligible up to temperatures of about 2250 °C [31]. However, it will readily react with oxygen, carbon, and silicon. Only purified source materials can be used and the preheating step must be performed under high vacuum conditions to remove residual oxygen. Thermal insulation is provided by tungsten heat shields; graphite insulation can be employed if not in direct contact, but severely degrades the crucible lifetime.

TaC is available as ceramic powder and can be sintered to 96 % vol density without sintering aids [38, 72]. TaC is chemically stable under AlN growth conditions at temperatures well exceeding 2300 °C. TaC elements are compatible with graphite (for susceptor and insulation elements), tungsten (possible use of TaC as susceptor) and SiC (as seeds), even if in direct contact. Long-term stability is generally limited by cracking due to internal grain growth [38]. To prevent structural failure, the crucible is commonly enclosed in graphite cylinders which also act as a susceptor [49]. As a variant, carburized tantalum crucibles can be employed [73]. However, as they are typically used with graphite parts, the crucibles continue to carburize and finally become brittle; this process is accelerated at growth temperatures exceeding 2100 °C. TaC coatings are no alternative as they tend to crack and spall off due to differences in thermal expansion and chemical attack.

The AlN source material is prepared from commercially available ceramic powder material by carbothermal reduction [74], sintering, or sublimation [75], while direct synthesis from high-purity elements [31] is less common. The purification process should remove the most important impurities and condense the source material to mitigate moisture adsorption during handling in air. Typical contamination of purified stating material is less than 100 ppm wt for oxygen and carbon, and about 2 ppm wt of silicon [75]. On the other hand, tungsten acts as a getter material for carbon and silicon. In contrast, TaC acts as a source of carbon, which leads to carbon contamination of the crystal and at the same time to a lower oxygen incorporation due to carbothermal reduction of residual oxides.

2.4 Seeded Growth and Crystal Enlargement

In the past, different technologies for seed preparation and crystal enlargement have been evaluated by different research groups [42]. In unseeded growth, crystals nucleate on the crucible lid, and a polycrystalline boule grows from which large grains can be separated. Grain selection is possible using a conical lid [31] or repeated regrowth [70]. However, grains are often strained or structurally deteriorated due to direct contact to their neighbors. Several groups reported growth of free-standing single crystals that spontaneously nucleated on crucible parts under conditions close to thermodynamic equilibrium and low nucleation density. Typically, tungsten grids are placed above the source material and the axial temperature gradients are lowered to the lowest possible value to yield optimum nucleation and growth conditions [76–78].

The growth rate of AlN is the slowest on prismatic facets for all but the highest growth temperatures, thus the crystal habit changes from needles to almost equiaxed (isometric) crystals [62, 78] with increasing temperature. The spontaneously nucleated crystals grown in carbon-free tungsten set-ups preferentially grow in Al-polar direction and show an unfinished habit, governed by pyramidal facets on the Al-polar side [76] and with only small (0001) basal plane facets (Fig. 2.3a). In contrast, crystals grown in TaC crucibles grow preferentially in N-polar directions, forming dominant (000-1) basal plane as well as prismatic side facets [78] (Fig. 2.3b, c). In each case, crystals nucleating in "wrong" directions become stunted and are easily overgrown by their neighbors. Single crystals with dimensions of up to 15 × 15 × 10 mm^3 have been obtained, which can be cut and used as seeds in subsequent growth runs. However, this process is not very reproducible and the yield of large and well-formed crystals is low.

Thick layers of AlN can be grown on SiC seeds, which are commercially available at industrial relevant sizes (4–6 in. in diameter). The fundamental disadvantage is the partial decomposition of SiC in the presence of AlN already at temperatures of 2000 °C, which contaminates the growing crystal with up to several atomic percent of silicon and carbon [79, 80]. Additionally, the mismatch of lattice

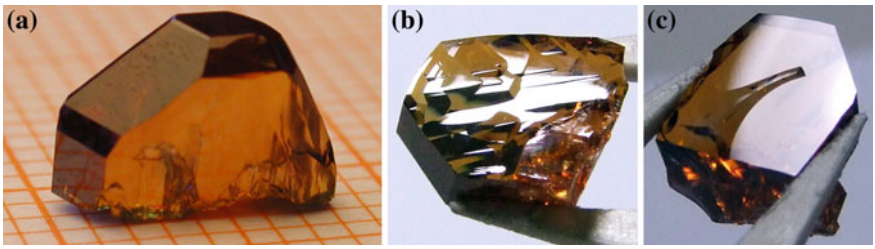

Fig. 2.3 Spontaneously nucleated, free-standing AlN bulk crystals; **a** grown in a tungsten crucible (on mm grid), the (0001)Al facet is upwards; **b**, **c** grown in a TaC crucible, crystal dimensions about 8 mm. **b** the Al-polar face is upwards but note that the (0001)Al-polar facet does not appear; **c** the flat (000-1)N facet is upwards

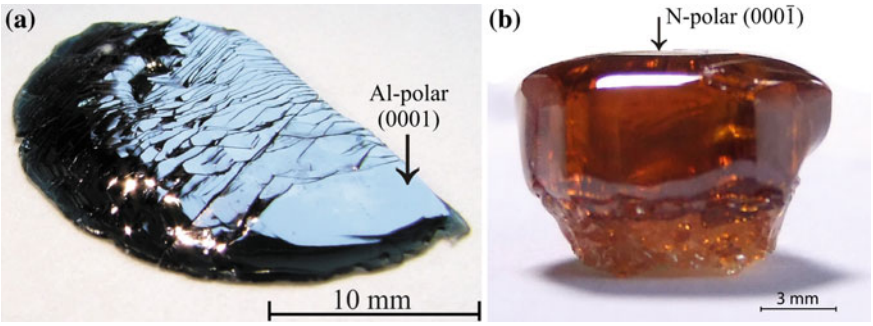

Fig. 2.4 **a** AlN crystal (Al-polar) grown on a SiC seed with 7° off-orientation with respect to the (0001) plane [82]; **b** AlN crystal (N-polar) grown on an N-polar (000-1) AlN seed [78]. Growth was performed in a TaC set-up, the crystals are turned so that the as-grown surface is upwards

parameters between AlN and SiC results in a formation of tilted domains, and the different thermal expansion coefficients lead to partial stress relaxation by dislocation formation during cooling, often resulting in a network of cracks originating at the interface [44, 81]. Nevertheless, the threading dislocation density between the domain boundaries may be as low as 10^5 cm^{-2} [82, 83]. A sample crystal is shown in Fig. 2.4a. AlN always grows Al-polar on polar SiC planes. These layers can be separated from the SiC seed and are used as seeds in subsequent AlN bulk growth [44, 45].

The main advantage of bulk crystal growth—steady improvement in diameter and structural quality—is only achieved in "homoepitaxial growth," i.e., wafers cut from the grown crystal are used as seeds in subsequent growth runs. Unfortunately, to grow a single crystal of a particular diameter, the seed must have roughly the same diameter. Seeded growth of AlN crystals has been successfully attempted from AlN seeds cut from spontaneously nucleated crystals as well as from AlN layers separated from SiC seeds. While in the former case, the main task is to perpetuate the high structural quality while providing for crystal enlargement, the latter approach is concerned with the defect density inherited from the seed and the impending diameter decrease due to formation of pyramidal side facets during Al-polar growth. Figure 2.4b shows a crystal grown on an N-polar basal plane seed with typical habit.

AlN growth is best performed on polar basal plane (c-plane) surfaces, because these planes possess isotropic in-plane properties. The ideal interface shape in sublimation growth is slightly convex, to allow the step flow from a single growth center (e.g., a screw dislocation to enable spiral growth) to spread across the whole surface area. AlN growth in other orientations has been reported [84–86], but the lower symmetry of the growth surface leads to anisotropic growth and formation of macrosteps and extended defects.

The major current issues in seeded growth of AlN are seed fixation, mitigation of seed backside evaporation, and preventing adjacent ("parasitic") grain growth. A rigid connection between the seed and the lid may lead to considerable strain,

formation of cracks, and potential seed separation from the lid during the heating-up stage due to the differences in thermal expansion. If the connection is too soft, the seed may move or fall down during the heating-up stage, and outer parts of the seed may evaporate due to the gap between the fixation rim and the lid. In any case, pores or gaps between the seed and the lid lead to seed backside evaporation. Material from the seed sublimes toward the colder crucible lid to close the void, and as a consequence, they travel through the seed and eventually through the growing crystal (negative crystal growth, cf. [87]) to locally degrade the crystal quality [86]. Seed backside plating [88] is a possible means to mitigate both backside evaporation and cracking. Nucleation and growth of parasitic grains, which also lead to strain and crystal cracking during cooling due to anisotropic thermal expansion of AlN, can be prevented by proper tailoring of the thermal field, i.e., increasing the temperature around the seed area.

2.5 Structural Defects in PVT-Grown AlN Bulk Crystals

As for any bulk growth method, the structural quality of the resulting bulk single crystals decisively depends on the seed quality and growth conditions. Defects from the seed volume and its surface as well as from backside areas of improper seed fixation penetrate into the growing crystal. A number of defects originate at the seed surface or form during initial stages of growth when the growth conditions are not yet stable. Defect formation during growth is caused by growth instabilities such as local variations of the supersaturation at the growth interface and thermal stress, and promoted by high temperatures and gradients, low pressures, and high growth rates. Finally, thermal stress during cooling may lead to formation of slip bands (consisting of straight rows of basal plane dislocations) [89] or even cracks [90] in the outer parts of the crystal.

Piercing points of dislocations, low angle grain boundaries (LAGBs), and inversion domains can be visualized by KOH–NaOH wet chemical etching on the Al-polar basal crystal surfaces and polished wafers [91, 92], see Fig. 2.5a. Another valuable detection method is X-ray topography [77, 93, 94], see Fig. 2.5b. In some samples, also cathodoluminescence imaging was successfully used [95]. Some of the threading screw dislocations act as growth centers for spiral growth. If their density is low, the resulting spirals may extend over several square millimeters and form hexagonal hillocks or round plateaus on the growth surface [45].

Spontaneously nucleated and free-standing crystals can be virtually unstrained and show highest structural perfection, i.e., overall dislocation densities below 10^3 cm^{-2} without any micropipes or volume defects [77, 78]. Rocking curve full width at half maximum (FWHM) values of 12–20 arcsecs are achieved even for large areas and in open detector measurements. The dislocation density in the crystals is typically very inhomogeneous, as basal plane dislocations mainly form due to local deformation, e.g., at the crystal border or at macrosteps (cf. Fig. 2.5b), while threading dislocations generally nucleate at growth instabilities or defects.

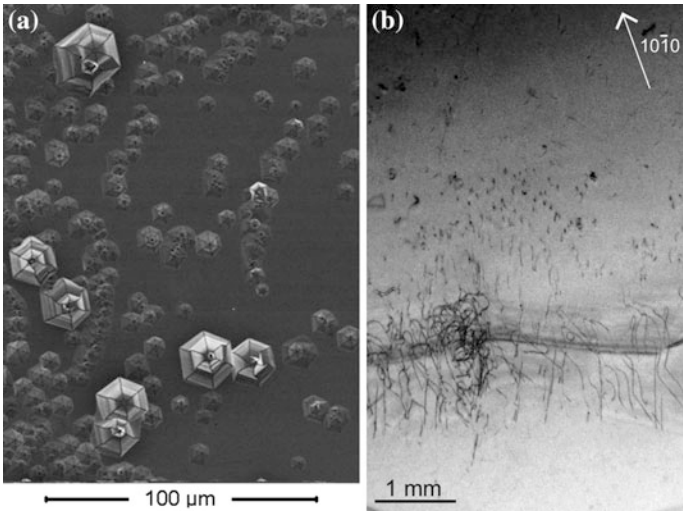

Fig. 2.5 Dislocations in AlN bulk crystals; **a** scanning electron microscope image of an Al-polar (0001) surface (seeded growth) after wet chemical etching. Bigger and smaller etch pits denote threading screw and mixed/edge dislocations, respectively; **b** X-ray transmission Lang topography image of a 1 mm thick basal plane wafer (spontaneously nucleated crystal) showing dark contrast from threading dislocations (*black dots*) and basal plane dislocations (*black curved lines*) partially entering a strained area (wavy interference contrast) caused by a macrostep formation at the growing surface. Note that the areas on the *bottom* and *top* of the image are virtually dislocation free

Additionally, in some of the earlier crystals a high density of microscopic inclusions were found, and these inclusions also decorated grown-in dislocations [93].

AlN bulk crystals often feature a mosaic structure, in particular when they were grown on defect-containing or foreign seeds. Several growth centers appearing at initial stages of growth lead to tilted domains after coalescence, eventually forming sub-grains bound by LAGBs composed of threading edge dislocations [94, 95]. If present, a mosaic structure of the seed also propagates into the growing crystal. The tilt between domains is typically below 100 arcsecs [1, 3], while growth on SiC seeds can lead to tilt values of up to 0.5° [83] and the formation of macroscopic hexagonal hillocks on the surface [45, 81]. Additional LAGBs may form in the outer crystal area during diameter enlargement where lateral expansion by growth on prismatic facets is accompanied by polygonization [96, 89]. The dislocation densities in AlN crystals grown on AlN seeds are typically in the 10^3–10^5 cm^{-2} range.

Inversion domains may be observed in particular in AlN crystals grown on SiC seeds [86, 97]. They nucleate probably due to growth instabilities and expand in size during further growth.

Finally, AlN bulk crystals exhibit a so-called zonar structure. Crystallographically different facets feature a different incorporation of impurities and thus, the corresponding crystal zones—i.e., crystal volume parts that were

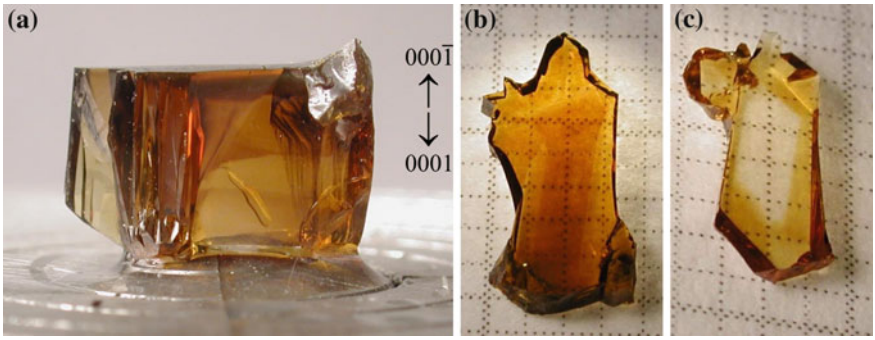

Fig. 2.6 Spontaneously nucleated, free-standing bulk AlN crystal with zonar structure, grown in a tungsten crucible; **a** side view, the N-polar basal plane is upwards; **b** top basal plane cut (on mm grid) showing crystal parts grown on the N-polar basal plane facet (*center region*) and on prismatic facets (*outer regions*); **c** bottom cut (on mm grid) showing crystal parts grown on the Al-polar basal facet (*center region*) and on Al-polar pyramidal facets (*outer regions*)

grown on the respective facets—show different optical (e.g., transmission and luminescence) and electrical properties. Due to obvious differences in coloration, the zones are easily distinguished in polished wafers [45, 78, 98] as shown in Fig. 2.6. Crystal zones are not bounded by LAGBs or other structural defects.

2.6 Impurities and Resulting Properties of AlN Substrates

Apart from size and structural quality, the key requirement for using AlN substrates for UV optoelectronics is high optical transmittance at the emission/detection wavelength. While AlN should be transparent for radiation above approximately 210 nm due to its band-gap of about 6.015 eV at room temperature [99], optical transitions involving deep levels lead to broad absorption bands in the blue and UV wavelength range. While it is recognized that these optical properties are induced by residual impurities such as carbon, silicon, and oxygen, the underlying mechanisms are still under discussion [31, 75, 100, 101, 102, 103, 104]. Apart from chemical analysis, the concentration of electrically active impurities of AlN bulk crystals has been evaluated from bound exciton luminescence [105, 106], electron paramagnetic resonance [104, 107, 108], infrared spectroscopy [103], and high-temperature resistivity measurements [75].

Due to the unavoidable contamination during high-temperature sublimation growth, the effects of different impurities can be hardly separated in optical absorption or luminescence spectra. Furthermore, intrinsic defects (such as vacancies) and defect clusters will enable additional optical transitions. The formation of such defects and their dependence on impurity incorporation is barely understood [109], and only a few techniques exist [110, 111] to evidence their concentrations. As a consequence, efforts to influence electrical and optical

properties of bulk AlN crystals are still focused on reducing contamination from both feedstock and set-up materials, rather than on controlled doping.

Oxygen is the main contamination of the source material and introduced to the growth chamber during loading/unloading in air. Silicon also occurs in the source material, although at lower levels compared to oxygen, and probably in the TaC hot-zone materials. Carbon is mainly introduced by the hot-zone materials such as the TaC crucible, the graphite susceptor, and graphite insulation parts. On the other hand, the impurity content in the crystals is strongly influenced by the materials in the hot-zone, by the crystal zone, i.e., the facet on which the impurity was incorporated. As a consequence, the oxygen and carbon concentrations of crystals grown in Al-polar direction in pure tungsten set-ups are considerably lower as compared to crystals grown in N-polar direction in TaC crucibles, see Table 2.1. Note that the formation of a zonar structure poses a problem when aiming at substrates with homogeneous absorption properties. Finally, the impurity content also depends on the growth temperature [75].

Figure 2.7 shows optical absorption (OA) spectra of the AlN crystals listed in Table 2.1. The broad OA band at around 2.8 eV which causes the yellowish coloration of the crystals is most dominant on the N-polar (000-1) zones. As it does not seem to correlate directly to a concentration of a single impurity, involvement of intrinsic defects is suspected [31, 100, 101]. A steep OA band at 4.7 eV, presumably consisting of several sub-peaks [112], dominates the spectra of crystals grown in TaC crucibles (and in particular crystals grown on SiC seeds, cf. [44, 79]). While this peak is clearly related to the carbon concentration in the crystal, the exact optical transitions that form this band are still under debate [45, 103, 113]. The band is absent in samples where the oxygen or silicon concentration clearly exceeds the carbon contamination, pointing toward a Fermi level effect. A monotonic OA increase above 5.3 eV is correlated to the 4.7 eV band, but in any case, the onset of near band-gap features limits the deep-UV transparency of AlN substrates effectively to wavelengths above about 220 nm. Finally, in some brownish areas, a broad band peaking around 4.0 eV is observed, presumably caused by oxygen and/or intrinsic defects [112].

Table 2.1 Typical values of impurity concentrations (in 10^{18} cm^{-3}) in different zones of bulk AlN crystals as measured by calibrated secondary ion mass spectrometry [123]

No.	Crucible	Zone	[O]	[Si]	[C]	References
1	W	Al-polar (0001)	0.4	0.20	0.7	[45]
2	W	Al-polar {10-13}	5.5	0.25	0.2	[45]
3	W	Al-polar {11-25}	5.0	0.7	3.5	[45]
4	W	Al-polar (0001)	2.0	0.01	0.5	[112]
5	W	Al-polar {10-12}	3.5	0.10	0.6	[112]
6	TaC	prismatic {10-10}	7.0	0.03	6.0	[78]
7	TaC	N-polar (000-1)	30	0.1	5.0	[78]
8	TaC	N-polar (000-1)	20	5.0	30	[114]

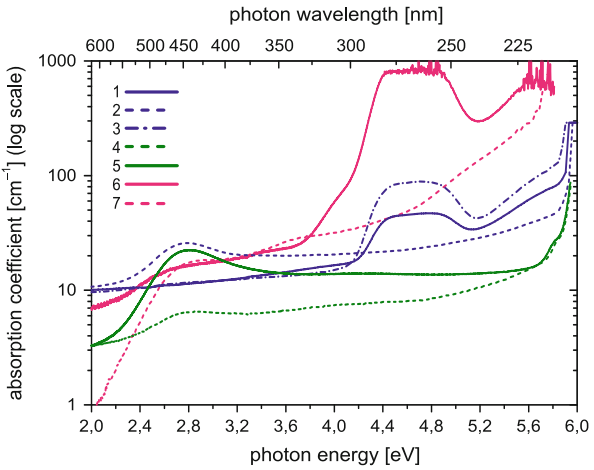

Fig. 2.7 Room temperature optical absorption spectra of selected bulk AlN crystals; the sample numbers correspond to the entries of Table 2.1 [122]

Especially the 4.7 eV absorption peak is detrimental to the light out-coupling of deep-UV (250–280 nm) emitters through the substrate. The best optical absorption values (without reflection corrections) for PVT-grown AlN published so far [112] are about 8 cm^{-1} on a local spot and about 13 cm^{-1} on a full wafer with yellowish coloration, both from a crystal grown in a pure tungsten set-up (No. 4 and 5 of Table 2.1, respectively). In contrast, AlN grown in TaC crucibles hardly shows absorption coefficients lower than 50 cm^{-1} at 265 nm (No. 7 of Table 2.1) [78]. As a consequence, the AlN substrate is thinned down to 20 µm after processing [50], or a HVPE thick layer (typically 250 µm) is deposited on the substrate and the substrate is subsequently removed by mechanical polishing [21]. The best reported optical absorption value for HVPE-grown AlN at 265 nm is 6.6 cm^{-1}, measured on a sample with the carbon and oxygen concentrations of below 0.2×10^{18} cm^{-3} and below 0.4×10^{18} cm^{-3}, respectively [114].

Using the above band-gap excitation, e.g., by an ArF excimer laser at 193 nm or by electron irradiation in an electron microscope, near band-gap emission can be observed. Excitonic luminescence recorded at low temperatures reveal valuable information about the material quality, e.g., strain and dislocation density. Furthermore, the intensity of the donor bound exciton emission corresponds to the respective donor (silicon, oxygen) concentration. However, as significant compensation by carbon quenches the excitonic luminescence, this technique has been successfully applied so far only to AlN bulk crystals grown pure in tungsten set-ups [106] or on homoepitaxial HPVE layers [105].

Below band-gap luminescence is very interesting for AlN ceramics in UV and ionization radiation dosimetry applications, but could also provide unwanted side effects in deep-UV emission devices. Ceramic samples, which are highly contaminated with oxygen and trace metals, show major luminescence bands at around 2.1 and 2.8 eV [115]. These bands are also observed in bulk AlN crystals, together with a band at 3.9 eV [45, 116]. The bands at 2.8 and 3.9 eV correlate to the carbon contamination in the samples [45, 113, 117]. The luminescence at 2.1 eV is found

in samples of very different provenance, and its origin currently remains unclear. On the other hand, luminescence in the 3.3–3.6 eV range clearly dominates the spectra of AlN either grown with SiC addition [79, 118] or in pure tungsten set-ups [98, 101, 119]. The common interpretation is that this band correlates to transitions of shallow donors (silicon or oxygen) to aluminum vacancies or their complexes [118, 120]. Obviously, these transitions are quenched as the carbon concentration exceeds that of the shallow donors.

AlN crystals and substrates are generally not electrically conductive. Measurements of the temperature-dependent conductivity show that the crystals are strongly compensated by deep levels with activation energies in the range of 0.6–1.0 eV [75, 121]. However, the different zones of the crystals show significant differences in charging after electron irradiation, e.g., in a scanning electron microscope [119]. Measurements of the temperature-dependent free carrier absorption indicate that carbon contamination may lead to semi-insulating behavior, while oxygen-dominated yellowish samples might show some very weak conductivity at elevated temperatures.

2.7 Conclusions and Outlook

Within the last 15 years, the growth of AlN bulk single crystals by the PVT method has matured from basic transport experiments yielding polycrystalline boules into an industrially applicable technique. Fueled by the interest in UV optoelectronics, the research has always aimed at providing material for substrates, with a clear focus on crystal size, process stability, and yield. Consequently, this progress was almost completely driven by appreciation of experimental work, i.e., solving technological issues such as finding compatible hot-zone materials, proper techniques for purification of the AlN starting material, and optimum growth conditions, as well as mitigating defect formation, backside evaporation, and parasitic nucleation.

While possible solutions to these issues are outlined in this chapter, important details remain proprietary technology based on the researchers' experimental knowledge. Each research team is bound to its developed technology, in particular the crucible material and the seeding/enlargement strategy. Teams that developed AlN on SiC seeds [44, 45, 49] have already demonstrated single crystals with 2 in. in diameter, but are faced with inhomogeneities and structural defects in the crystals, as well as problems in keeping the diameter in subsequent growth runs. On the other hand, teams that focused on AlN grain enlargement while perpetuating the high structural quality [77, 78] have been able to increase the single-crystalline diameter by only about 3 mm/year on average.

This poses at least two serious implications for future development of AlN crystals and substrates: First, the number of parties able to provide state-of-the-art substrates will remain limited, as newcomers lack the experimental experience. Second, technology convergence as well as further progress and commercial

breakthrough will decisively depend on further improvements in understanding the AlN growth technology, in particular regarding the influence of contaminants and dopants on crystal growth. Finally, the high temperatures and low growth rates of AlN PVT growth will limit the use of AlN substrates to applications which clearly benefit from the unique properties of this material. As it stands, deep-UV opto-electronics is one of them.

Acknowledgments The author acknowledges contributions of J. Wollweber, C Hartmann, A. Dittmar, K. Irmscher, T. Schulz, F. Langhans, S. Kollowa, C. Guguschev, M. Pietsch, A. Kwasniewski, M. Albrecht, M. Naumann, T. Neugut, and U. Juda from the Leibniz Institute for Crystal Growth. The author also thanks B.M. Epelbaum, O. Filip, P. Heimann, and A. Winnacker for the joint work on bulk AlN growth at the Department of Materials Science 6, University of Erlangen-Nuremberg, Germany, now continued in the company CrystAl-N.

References

1. R. Dalmau, B. Moody, R. Schlesser, S. Mita, J. Xie, M. Feneberg, B. Neuschl, K. Thonke, R. Collazo, A. Rice, J. Tweedie, Z. Sitar, J. Electrochem. Soc. **158**, H530 (2011)
2. J. Tweedie, R. Collazo, A. Rice, J. Xie, S. Mita, R. Dalmau, Z. Sitar, J. Appl. Phys. **108**, 043526 (2010)
3. R.T. Bondokov, S.G. Mueller, K.E. Morgan, G.A. Slack, S. Schujman, M.C. Wood, J.A. Smart, L.J. Schowalter, J. Cryst. Growth **310**, 4020 (2008)
4. L.H. Dreger, V.V. Dadape, J.L. Margrave, J. Phys. Chem. **66**, 1556 (1962)
5. M. Levinshtein, S. Ruymantsev, M. Shur (eds.), *Properties of Advanced Semiconductor Materials, GaN, AlN, InN, BN, SiC, SiGe* (Wiley, New York, 2001). ISBN 978-0-471-35827-5
6. G.A. Slack, J. Phys. Chem. Solids **34**, 321 (1973)
7. G.A. Slack, T.F. McNelly, J. Cryst. Growth **34**, 263 (1976)
8. T. Baker, A. Mayo, Z. Veisi, P. Lu, J. Schmitt, Phys. Status Solidi C **11**, 373 (2014)
9. O. Kovalenkov, V. Soukhoveev, V. Ivantsov, A. Usikov, V. Dmitriev, J. Cryst. Growth **281**, 87 (2005)
10. Y. Katagiri, S. Kishino, K. Okuura, H. Miyake, K. Hiramatu, J. Cryst. Growth **311**, 2831 (2009)
11. Y. Kumagai, J. Tajima, M. Ishizuki, T. Nagashima, H. Murakami, K. Takada, A. Koukitu, Appl. Phys. Express **1**, 045003 (2008)
12. J.A. Freitas Jr, G.C.B. Braga, E. Silveira, J.G. Tischler, M. Fatemi, Appl. Phys. Lett. **83**, 2584 (2003)
13. T. Furusho, S. Ohshima, S. Nishino, Mater. Sci. Forum **389–393**, 1449 (2002)
14. R. Schlesser, Z. Sitar, J. Cryst. Growth **234**, 349 (2002)
15. K. Kamei, Y. Shirai, T. Tanaka, N. Okada, A. Yauchi, H. Amano, Phys. Status Solidi C **4**, 2211 (2007)
16. M. Bockowski, Cryst. Res. Technol. **36**, 771 (2001)
17. M. Yano, M. Okamoto, Y.K. Yap, M. Yoshimura, Y. Mori, T. Sasaki, Diam. Relat. Mater. **9**, 512 (2000)
18. Y. Kangawa, R. Toki, T. Yayama, B.M. Epelbaum, K. Kakimoto, Appl. Phys. Express **4**, 095501 (2011)
19. B.T. Adekore, K. Rakes, B. Wang, M.J. Callahan, S. Pendurti, Z. Sitar, J. Electron. Mater. **35**, 1104 (2006)

20. R. Dwilinski, R. Doradzinski, J. Garczynski, L. Sierzputowski, M. Palczewska, A. Wysmolek, M. Kaminska, MRS Internet J. Nitride Semicond. Res. **3**, 1 (1998)
21. T. Kinoshita, K. Hironaka, T. Obata, T. Nagashima, R. Dalmau, R. Schlesser, B. Moody, J. Xie, S.-I. Inoue, Y. Kumagai, A. Koukitu, Z. Sitar, Appl. Phys. Express **5**, 122101 (2012)
22. Fr. Briegleb, A. Geuther, Justus Liebigs Ann. Chem. **123**, 228 (1877)
23. W. Nakao, H. Fukuyama, K. Nagata, J. Am. Ceram. Soc. **84**, 889 (2002)
24. W. Werdecker, F. Aldinger, I.E.E.E. Trans, Hybrids Manuf. Technol. **7**, 399 (1984)
25. L.M. Sheppard, Am. Ceram. Soc. Bull. **69**, 1801 (1990)
26. G.A. Slack, M.R.S. Symp, Proc. **512**, 35 (1998)
27. K.M. Taylor, C. Lenie, J. Electrochem. Soc. **107**, 308 (1960)
28. H.-D. Witzke, Phys. Status Solidi **2**, 1109 (1962)
29. J. Pastrnak, L. Roskovcova, Phys. Status Solidi **7**, 331 (1964) (in German)
30. G.A. Cox, D.O. Cummins, K. Kawabe, R.H. Tredgold, J. Phys. Chem. Solids **28**, 543 (1967)
31. G.A. Slack, T.F. McNelly, J. Cryst. Growth **42**, 560 (1977)
32. G.A. Slack, *Aluminum Nitride Crystal Growth,* U.S. Air Force Office of Scientific Research (1979). DTIC document ADA085932 (http://www.dtic.mil)
33. W.W. Piper, S.J. Polich, J. Appl. Phys. **32**, 1278 (1961)
34. C.M. Balkas, Z. Sitar, T. Zheleva, L. Bergman, R. Nemanich, R.F. Davis, J. Cryst. Growth **179**, 363 (1997)
35. M. Tanaka, S. Nakahata, K. Sogabe, H. Nakata, M. Tobioka, Jpn. J. Appl. Phys. **36**, L1062 (1997)
36. J.C. Rojo, G.A. Slack, K. Morgan, B. Raghothamachar, M. Dudley, L.J. Schowalter, J. Cryst. Growth **231**, 317 (2001)
37. Yu.M. Tairov, Mater. Sci. Eng. B **29**, 83 (1995)
38. R. Schlesser, R. Dalmau, D. Zhuang, R. Collazo, Z. Sitar, J. Cryst. Growth **281**, 75 (2005)
39. R. Dalmau, B. Raghothamachar, M. Dudley, R. Schlesser, Z. Sitar, MRS Symp. Proc. **798**, Y2.9 (2004)
40. B. Liu, J.H. Edgar, Z. Gu, D. Zhuang, B. Raghothamachar, M. Dudley, A. Sarua, M. Kuball, H.M. Meyer III, MRS Internet J. Nitride Semicond. Res. **9**, 6 (2004)
41. G.A. Slack, J. Whitlock, K. Morgan, L.J. Schowalter, MRS Symp. Proc. **798**, Y10.74 (2004)
42. B.M. Epelbaum, M. Bickermann, A. Winnacker, J. Cryst. Growth **275**, e479 (2005)
43. S.G. Mueller, R.T. Bondokov, K.E. Morgan, G.A. Slack, S.B. Schujman, J. Grandusky, J.A. Smart, L.J. Schowalter, Phys. Status Solidi A **206**, 1153 (2009)
44. R.R. Sumathi, P. Gille, Jpn. J. Appl. Phys. **52**, 08JA02 (2013)
45. M. Bickermann, B.M. Epelbaum, O. Filip, B. Tautz, P. Heimann, A. Winnacker, Phys. Status Solidi C **9**, 449 (2012)
46. Z.G. Herro, D. Zhuang, R. Schlesser, Z. Sitar, J. Cryst. Growth **312**, 2519 (2010)
47. I. Nagai, T. Kato, T. Miura, H. Kamata, K. Naoe, K. Sanada, H. Okumura, J. Cryst. Growth **312**, 2699 (2010)
48. M. Miyanaga, N. Mizuhara, T. Kawase, S. Fujiwara, M. Shimazu, H. Nakahata, T. Kawase, J. Cryst. Growth **300**, 45 (2007)
49. Yu.N. Makarov, O.V. Avdeev, I.S. Barash, D.S. Bazarevskiy, T.Yu. Chemekova, E.N. Mokhov, S.S. Nagalyuk, A.D. Roenkov, A.S. Segal, Yu.A. Vodakov, M.G. Ramm, S. Davis, G. Huminic, H. Helava, J. Cryst. Growth **310**, 881 (2008)
50. J.R. Grandusky, J. Chen, S.R. Gibb, M.C. Mendrick, C.G. Moe, L. Rodak, G.A. Garrett, M. Wraback, L.J. Schowalter, Appl. Phys. Express **6**, 032101 (2013)
51. R. Collazo, S. Mita, J. Xie, A. Rice, J. Tweedie, R. Dalmau, Z. Sitar, Phys. Status Solidi C **8**, 2031 (2011)
52. T. Wunderer, C.L. Chua, Z. Yang, J.E. Northrup, N.M. Johnson, G.A. Garrett, H. Shen, M. Wraback, Appl. Phys. Express **4**, 092101 (2011)
53. M. Kneissl, Z. Yang, M. Teepe, C. Knollenberg, O. Schmidt, P. Kiesel, N.M. Johnson, S. Schujman, L.J. Schowalter, J. Appl. Phys. **101**, 123103 (2007)

54. M. Martens, F. Mehnke, C. Kuhn, C. Reich, V. Kueller, A. Knauer, C. Netzel, C. Hartmann, J. Wollweber, J. Rass, T. Wernicke, M. Bickermann, M. Weyers, M. Kneissl, IEEE Photonics Lett. **26**, 342 (2014)
55. J. Xie, S. Mita, Z. Bryan, W. Guo, L. Hussey, B. Moody, R. Schlesser, R. Kirste, M. Gerhold, R. Collazo, Z. Sitar, Appl. Phys. Lett. **102**, 171102 (2013)
56. T. Erlbacher, M. Bickermann, B. Kallinger, E. Meissner, A.J. Bauer, L. Frey, Phys. Status Solidi C **9**, 968 (2012)
57. G. Bu, D. Ciplys, M. Shur, L.J. Schowalter, S. Schujman, R. Gaska, IEEE Trans. Ultrasonics Ferroelectr. Freq. Control **53**, 251 (2006)
58. X. Hu, J. Deng, N. Pala, R. Gaska, M.S. Shur, C.Q. Chen, J. Yang, G. Simin, M.A. Khan, J. C. Rojo, L.J. Schowalter, Appl. Phys. Lett. **82**, 1299 (2003)
59. A. Dobrinsky, G. Simin, R. Gaska, M. Shur, ECS Trans. **58**(4), 129 (2013)
60. L. Siang-Chung, Mater. Sci. Lett. **16**, 759 (1997)
61. Y. Li, D.W. Brenner, Phys. Rev. Lett. **92**, 075503 (2004)
62. B.M. Epelbaum, M. Bickermann, S. Nagata, P. Heimann, O. Filip, A. Winnacker, J. Cryst. Growth **305**, 317 (2007)
63. V. Noveski, R. Schlesser, S. Mahajan, S. Beaudoin, Z. Sitar, J. Cryst. Growth **264**, 369 (2004)
64. Q.-S. Chen, V. Prasad, H. Zhang, M. Dudley, in: K. Byrappa, T. Ohachi (eds.), *Crystal Growth Technology* (Springer, Berlin, 2005). ISBN 978-3-540-00367-0, chap. 7
65. S.Yu. Karpov, D.V. Zimina, Yu.N. Makarov, E.N. Mokhov, A.D. Roenkov, M.G. Ramm, Yu.A. Vodakov, Phys. Status Solidi A **176**, 435 (1999)
66. A.S. Segal, S.Yu. Karpov, Yu.N. Makarov, E.N. Mokhov, A.D. Roenkov, M.G. Ramm, Yu. A. Vodakov, J. Cryst. Growth **211**, 68 (2000)
67. P. Heimann, B.M. Epelbaum, M. Bickermann, S. Nagata, A. Winnacker, Phys. Status Solidi C **3**, 1575 (2006)
68. S.Yu. Karpov, A.V. Kulik, I.N. Przhevalskii, M.S. Ramm, Yu.N. Makarov, Phys. Status Solidi C 0 1989 (2003)
69. M. Albrecht, J. Wollweber, M. Rossberg, M. Schmidbauer, C. Hartmann, R. Fornari, Appl. Phys. Lett. **88**, 211904 (2006)
70. Z.G. Herro, D. Zhuang, R. Schlesser, R. Collazo, Z. Sitar, J. Cryst. Growth **286**, 205 (2006)
71. M. Bickermann, B.M. Epelbaum, A. Winnacker, Phys. Status Solidi C **2**, 2044 (2005)
72. A. Dittmar, C. Guguschev, C. Hartmann, S. Golka, A. Kwasniewski, J. Wollweber, R. Fornari, J. Eur. Ceram. Soc. **31**, 2733 (2011)
73. C. Hartmann, J. Wollweber, M. Albrecht, I. Rasin, Phys. Status Solidi C **3**, 1608 (2006)
74. C. Guguschev, A. Dittmar, E. Moukhina, C. Hartmann, S. Golka, J. Wollweber, M. Bickermann, R. Fornari, J. Cryst. Growth **360**, 185 (2012)
75. M. Bickermann, B.M. Epelbaum, A. Winnacker, J. Cryst. Growth **269**, 432 (2004)
76. B.M. Epelbaum, C. Seitz, A. Magerl, M. Bickermann, A. Winnacker, J. Cryst. Growth **265**, 577 (2004)
77. B. Raghothamachar, J. Bai, M. Dudley, R. Dalmau, D. Zhuang, Z. Herro, R. Schlesser, Z. Sitar, B. Wang, M. Callahan, K. Rakes, P. Konkapaka, M. Spencer, J. Cryst. Growth **287**, 349 (2006)
78. C. Hartmann, J. Wollweber, A. Dittmar, K. Irmscher, A. Kwasniewski, F. Langhans, T. Neugut, M. Bickermann, Jpn. J. Appl. Phys. **52**, 08JA06 (2013)
79. M. Bickermann, O. Filip, B.M. Epelbaum, P. Heimann, M. Feneberg, B. Neuschl, K. Thonke, E. Wedler, A. Winnacker, J. Cryst. Growth **339**, 13 (2012)
80. R.R. Sumathi, P. Gille, Cryst. Res. Technol. **47**, 237 (2012)
81. O. Filip, B.M. Epelbaum, M. Bickermann, P. Heimann, S. Nagata, A. Winnacker, Mater. Sci. Forum **615–617**, 983 (2009)
82. C. Hartmann, M. Albrecht, J. Wollweber, J. Schuppang, U. Juda, Ch. Guguschev, S. Golka, A. Dittmar, R. Fornari, J. Cryst. Growth **344**, 19 (2012)
83. M. Bickermann, B.M. Epelbaum, O. Filip, P. Heimann, S. Nagata, A. Winnacker, Phys. Status Solidi C **5**, 1502 (2008)

84. B.M. Epelbaum, M. Bickermann, A. Winnacker, Mater. Sci. Forum **433–436**, 983 (2003)
85. D. Zhuang, Z.G. Herro, R. Schlesser, Z. Sitar, J. Cryst. Growth **287**, 372 (2006)
86. O. Filip, B.M. Epelbaum, M. Bickermann, P. Heimann, A. Winnacker, J. Cryst. Growth **318**, 427 (2011)
87. D. Hofmann, M. Bickermann, W. Hartung, A. Winnacker, Mater. Sci. Forum **338–342**, 445 (2000)
88. H. Helava, E.N. Mokhov, O.A. Avdeev, M.G. Ramm, D.P. Litvin, A.V. Vasiliev, A.D. Roenkov, S.S. Nagalyuk, Yu.N. Makarov, Mater. Sci. Forum **740–742**, 85 (2013)
89. R. Dalmau, B. Moody, J. Xie, R. Collazo, Z. Sitar, Phys. Status Solidi A **208**, 1545 (2011)
90. R.T. Bondokov, K.E. Morgan, R. Shetty, W. Liu, G.A. Slack, M. Goorsky, L.J. Schowalter, MRS Symp. Proc. **892**, FF30-03 (2006)
91. D. Zhuang, J.H. Edgar, Mater. Sci. Eng. R **48**, 1 (2005)
92. M. Bickermann, S. Schmidt, B.M. Epelbaum, P. Heimann, S. Nagata, A. Winnacker, J. Cryst. Growth **300**, 299 (2007)
93. B. Raghothamachar, M. Dudley, J.C. Rojo, K. Morgan, L.J. Schowalter, J. Cryst. Growth **250**, 244 (2003)
94. B. Raghothamachar, Y. Yang, R. Dalmau, B. Moody, S. Craft, R. Schlesser, M. Dudley, Z. Sitar, Mater. Sci. Forum **740–742**, 91 (2013)
95. M. Bickermann, S. Schimmel, B.M. Epelbaum, O. Filip, P. Heimann, S. Nagata, A. Winnacker, Phys. Status Solidi C **8**, 2235 (2011)
96. R.T. Bondokov, K.E. Morgan, R. Shetty, W. Liu, G.A. Slack, M. Goorsky, L.J. Schowalter, MRS Symp. Proc. **892**, FF30-03 (2006)
97. R. Dalmau, R. Schlesser, Z. Sitar, Phys. Status Solidi C **2**, 2036 (2005)
98. M. Bickermann, P. Heimann, B.M. Epelbaum, Phys. Status Solidi C **3**, 1902 (2006)
99. M. Feneberg, R.A.R. Leute, B. Neuschl, K. Thonke, M. Bickermann, Phys. Rev. B **82**, 075208 (2010)
100. G.A. Slack, L.J. Schowalter, D. Morelli, J.A. Freitas Jr, J. Cryst. Growth **246**, 287 (2002)
101. M. Bickermann, B.M. Epelbaum, O. Filip, P. Heimann, S. Nagata, A. Winnacker, Phys. Status Solidi B **246**, 1181 (2009)
102. L. Gordon, J.L. Lyons, A. Janotti, C.G. Van de Walle, Phys. Rev. B **89**, 085204 (2014)
103. K. Irmscher, C. Hartmann, C. Guguschev, M. Pietsch, J. Wollweber, M. Bickermann, J. Appl. Phys. **114**, 123505 (2013)
104. N.T. Son, M. Bickermann, E. Janzén, Appl. Phys. Lett. **98**, 092104 (2011)
105. B. Neuschl, K. Thonke, M. Feneberg, S. Mita, X. Xie, R. Dalmau, R. Collazo, Z. Sitar, Phys. Status Solidi B **249**, 511 (2012)
106. M. Feneberg, R.A.R. Leute, B. Neuschl, K. Thonke, M. Bickermann, Phys. Rev. B **82**, 075208 (2010)
107. S.B. Orlinskii, J. Schmidt, P. Baranov, M. Bickermann, B.M. Epelbaum, A. Winnacker, Phys. Rev. Lett. **100**, 256404 (2008)
108. S.M. Evans, N.C. Giles, L.E. Halliburton, G.A. Slack, S.B. Shujman, L.J. Schowalter, Appl. Phys. Lett. **88**, 062112 (2006)
109. C. Stampfl, C.G. van de Walle, Phys. Rev. B **65**, 155212 (2002)
110. N.T. Son, A. Gali, Á. Szabó, M. Bickermann, T. Ohshima, J. Isoya, E. Janzén, Appl. Phys. Lett. **98**, 242116 (2011)
111. F. Tuomisto, J.-M. Mäki, T.Yu. Chemekova, Yu.N. Makarov, O.V. Avdeev, E.N. Mokhov, A.S. Segal, M.G. Ramm, S. Davis, G. Huminic, H. Helava, M. Bickermann, B.M. Epelbaum, J. Cryst. Growth **310**, 3998 (2008)
112. M. Bickermann, B.M. Epelbaum, O. Filip, P. Heimann, S. Nagata, A. Winnacker, Phys. Status Solidi C **7**, 21 (2010)
113. R. Collazo, J. Xie, B.E. Gaddy, Z. Bryan, R. Kirste, M. Hoffmann, R. Dalmau, B. Moody, Y. Kumagai, T. Nagashima, Y. Kubota, T. Kinoshita, A. Koukitu, D.L. Irving, Z. Sitar, Appl. Phys. Lett. **100**, 191914 (2012)
114. T. Nagashima, Y. Kubota, T. Kinoshita, Y. Kumagai, J. Xie, R. Collazo, H. Murakami, H. Okamoto, A. Koukitu, Z. Sitar, Appl. Phys. Express **5**, 125501 (2012)

115. L. Trinkler, B. Berzina, in: *Advances in Ceramics: Characterization, Raw Materials, Processing, Properties, Degradation and Healing*, C. Sikalidis (ed.), InTech Open Access Book (2011). ISBN 978-953-307-504-4, chap. 4
116. A. Sedhain, L. Du, J.H. Edgar, J.Y. Lin, H.X. Jiang, Appl. Phys. Lett. **95**, 262104 (2009)
117. B.E. Gaddy, Z. Bryan, I. Bryan, R. Kirste, J. Xie, R. Dalmau, B. Moody, Y. Kumagai, T. Nagashima, Y. Kubota, T. Kinoshita, A. Koukitu, Z. Sitar, R. Collazo, D.L. Irving, Appl. Phys. Lett. **103**, 161901 (2013)
118. T. Schulz, M. Albrecht, K. Irmscher, C. Hartmann, J. Wollweber, R. Fornari, Phys. Status Solidi B **248**, 1513 (2011)
119. M. Bickermann, B.M. Epelbaum, O. Filip, P. Heimann, M. Feneberg, S. Nagata, A. Winnacker, Phys. Status Solidi C **7**, 1743 (2010)
120. T. Mattila, R.M. Nieminen, Phys. Rev. B **55**, 9571 (1997)
121. K. Irmscher, T. Schulz, M. Albrecht, C. Hartmann, J. Wollweber, R. Fornari, Phys. B **401–402**, 323 (2007)
122. Note that the absorption spectra for samples 6 and 7 differ to the ones shown in [78], as they were measured on similar crystals with virtually the same impurity concentrations. Furthermore, absorption coefficients above 700 cm^{-1} (sample 6) contain measurement artifacts
123. The silicon concentrations of samples 1 through 7 are corrected to reflect a calibration error which was found after the values cited in the references [75,78,112] had been published